Journal of Environmental Health Science and Engineering (2019) 17:873–888
https://doi.org/10.1007/s40201-019-00405-7

RESEARCH ARTICLE

Modeling and optimizing parameters affecting hexavalent chromium adsorption from aqueous solutions using Ti-XAD7 nanocomposite: RSM-CCD approach, kinetic, and isotherm studies

Sahar Sharifi[1] · Ramin Nabizadeh[1,2] · Bahman Akbarpour[1] · Ali Azari[3,4,5] · Hamid Reza Ghaffari[6] · Shahrokh Nazmara[1] · Babak Mahmoudi[1] · Leila Shiri[1] · Mahmood Yousefi[7]

Received: 26 May 2019 / Accepted: 26 September 2019 / Published online: 11 December 2019

Abstract

Background Due to the high toxicity of chromium, particularly as Hexavalent chromium Cr (VI), it is removed from industrial effluents before their discharge into the environment by a variety of methods, including loading catalysts onto the polymeric supports. This study focused on the removal of Cr(VI) from aqueous solutions using Amberlite XAD7 resin loaded titanium dioxide (Ti-XAD7).

Methods Ti-XAD7 was synthesized using Amberlite XAD-7 impregnated with titanium tetraethoxide. The prepared Ti-XAD7 was characterized by using Fourier transform infrared spectroscopy (FTIR), scanning electron microscopy (SEM) and X-ray diffraction (XRD). Isotherms and kinetic studies were carried out to describe the adsorption behavior of adsorbent for the removal of Cr(VI) ions. Quadratic models considering independent variables, i.e. the initial Cr(VI) concentration, adsorbent dosage, time, and pH, were evaluated and optimized to describe the behavior of Cr(VI) adsorption onto the Ti-XAD7 using RSM based on a Five-level-four-factor CCD approach.

Results The accuracy and the fitting of the model were evaluated by ANOVA with $R^2 > 0.725$ and P value $= 5.221 \times 10^{-5}$. The optimum conditions for the adsorption process were an initial Cr(VI) concentration 2750 ppb, contact time of 51.53 min, pH of 8.7, and Ti-XAD7 dosage of 5.05 g/L. The results revealed that the Langmuir and Sips isotherm models with $R^2 = 0.998$ and 0.999 were *the best models fitting* the *experimental data.* The adsorption capacity of Ti-XAD7 and R_L constant were 2.73 mg/g and 0.063–0.076 based on the Langmuir isotherm, respectively. Kinetic studies also indicated that the adsorption behavior of Cr(VI) was acceptably explained by the Elovich kinetic model with a good fitting ($R^2 = 0.97$).

Conclusions Comparison of the Ti-XAD7 and XAD7 yield in chromium adsorption showed that modified XAD7 had higher removal efficiency (about 98%) compared to XAD7 alone.

Keywords Cr(VI) adsorption · Ti-XAD7 · RSM statistical modeling · Process optimization · Isotherm and kinetic study

Nomenclature

ANOVA	Analysis of Variance
CCD	Central composite design
Cr(VI)	Hexavalent chromium.
C_0	Initial concentration of chromium solution (mg/L)
C_e	Equilibrium concentration of chromium solution (mg/L)
FTIR	Fourier-transform infrared spectroscopy

✉ Ramin Nabizadeh
rnabizadeh@tums.ac.ir; rnabizadeh@gmail.com

[1] Department of Environmental Health Engineering, School of Public Health, Tehran University of Medical Sciences, Tehran, Iran

[2] Center for Air Quality Research, Institute for Environmental Research (IER), Tehran University of Medical Sciences, Tehran, Iran

[3] Department of Environmental Health Engineering, School of Public Health, Kashan University of Medical Sciences, Kashan, Iran

[4] Research Center for Health, Safety and Environment (RCHSE), Alborz University of Medical Sciences, Karaj, Iran

[5] Students' Scientific Research Center (SSRC), Tehran University of Medical Sciences, Tehran, Iran

[6] Food Health Research Center, Hormozgan University of Medical Sciences, Bandar Abbas, Iran

[7] Department of Environmental Health Engineering, School of Public Health, Iran University of Medical Sciences, Tehran, Iran

GooF	Good of fitness
LOF	Lack of fit
RSM	Response surface methodology
SEM	Scanning electron microscope
XRD	X-ray diffraction
SNE	Sum of the normalized error
TWP	Two-parameter
THP	Three-parameter
V	Volume of chromium solution (mL)
W	Weight of the adsorbent (g)
X1	pH (dimensionless)
X2	Adsorbent dose (g/L)
X3	Time (min)
X4	Initial concentration of chromium (ppb)

Introduction

Industrial activities such as electroplating, welding, leather tanning, mining, dyeing, fertilizer, photography, and chromate painting processes discharge heavy metals like hexavalent chromium (Cr(VI)) into the environment through their effluents [1, 2]. Cr(VI) is one of the 17 humans threating chemicals identified by the U.S. Environmental Protection Agency (USEPA) due to its high toxicity, carcinogenicity, mutagenicity, solubility, and mobility in aqueous solutions [3–5]. US.EPA has set a maximum contaminant level of 10 μg L^{-1} for Cr(VI) in the drinking water and a range of 0.1–0.5 mg L^{-1} in the wastewater discharge [6, 7]. Thus, it is necessary to remove Cr(VI) from the wastewater before discharge into the environment. Recently, some methods including adsorption [8–12], biosorption [13], precipitation [14], electrocoagulation [15], photocatalytic reduction [16] and ion exchange [17, 18] have been developed for Cr(VI) removal from aqueous solutions. In the past decades, several studies showed that the combining the properties (characteristics) of the two methods, i.e. ion exchange with solvent extraction, led to the development of extractant-impregnated resins, which is a promising and suitable technique for adsorption of pollutants from aquatic environments [19, 20] . Amberlite XAD series, as part of the available commercial resins, are widely used for the impregnation process. This type of resin has interested researchers for its good physical properties such as high porosity, uniform pore size distribution, large surface area, and durability as well as a chemically homogeneous nonionic structure. So far, modification of Amberlite resins with various compounds, i.e. metal oxides, has been reported for separation of heavy metals from aqueous solutions [21–25]. Among different types of metal oxides used for removal of pollutants and heavy metals from wastewater, TiO_2 has shown promising results [26, 27]. Non-toxicity, low costs, inertness, flexibility in combination with other materials, and biocompatibility have made Titania compounds (TiO_2) an attractive material in various purification systems [28, 29]. In this regards, Zhang et al. [30] investigated the effect of titania loading on carbon black for Cr(VI) removal from aqueous solutions and reported that impregnation of titanium dioxide on carbon black can improve the performance of the adsorption process. According to the above, this study was conducted to evaluate impregnation of TiO_2 nanoparticles onto the Amberlite XAD7 resin and its characterization, to examine the efficiency of Ti-XAD7 nanocomposite in Cr(VI) adsorption considering the effects of operating parameters including adsorbent dose, contact time, pH, and initial Cr(VI) concentration using response surface methodology (RSM) as statistical approach, to predict and optimize the parameters affecting Cr(VI) adsorption by central composite design (CCD), and to evaluate the kinetics and the adsorption isotherms of Cr(VI).

Materials and methods

Chemicals and instruments

All chemicals, including Amberlite XAD-7 resin (mean particle size: 20–60 mesh), potassium dichromate ($K_2Cr_2O_7$, MW = 294.18), and titanium tetraethoxide, were purchased from Sigma-Aldrich (St. Louis, MO) and used without further purification. Double distilled water was used to prepare the Cr(VI) stock solution and dilution. Other required Cr(VI) concentrations for adsorption experiments were obtained by diluting the stock solution. Inductively coupled plasma optical emission spectrometry (ICP-OES) (ARCOS, SPECTRO®, Analytical Instrument, Kleve, Germany) was used for measurement of Cr(VI) absorbance. The prepared Ti-XAD7 was characterized by Scanning Electron Microscopy (SEM) (MIRA III, TESCAN®, Czech), Fourier Transform Infrared Spectroscopy (FTIR) (Avatar, Thermo®, USA), and XRD (PW1730, Philips®, Netherlands) techniques. pH was adjusted using a MITEC-965 (micra®, India) pH meter. A thermostatic shaker (Innova 4340, Eppendorf, Germany) was used for appropriate mixing of samples.

Preparation of Ti-XAD7

Prior to the impregnation process, Amberlite XAD-7 resin was washed with double distilled water and dried in an oven at 200 °C for 120 min [31]. Ti-XAD7 was synthesized using Amberlite XAD-7 impregnated with titanium tetraethoxide. For this purpose, 21 g of dried resin was

Table 1 CCD Matrix for adsorption experiments of Cr(VI) onto the Ti-XAD7

Name	Coded variable	Units	- α	-1	0	+1	+ α
Solution pH	X_1	–	3	5.25	7.5	9.75	12
Adsorbent dosage	X_2	g/L	0.1	2.575	5.05	7.525	10
Contact time	X_3	min	5	26.25	47.5	68.75	90
Cr(VI) concentration	X_4	ppb	500	1625	2750	3875	5000
Run	pH		Adsorbent dose		Contact time		Cr(VI) concentration
1	7.5		5.05		47.5		2750
2	9.75		7.525		26.25		1625
3	9.75		7.525		26.25		3875
4	9.75		7.525		68.75		3875
5	5.25		2.575		26.25		1625
6	9.75		2.575		68.75		1625
7	5.25		7.525		26.25		3875
8	7.5		5.05		47.5		2750
9	9.75		2.575		26.25		3875
10	7.5		5.05		47.5		2750
11	5.25		7.525		26.25		1625
12	7.5		5.05		47.5		2750
13	5.25		2.575		68.75		1625
14	5.25		2.575		68.75		3875
15	9.75		2.575		68.75		3875
16	9.75		2.575		26.25		1625
17	5.25		7.525		68.75		3875
18	7.5		5.05		47.5		2750
19	7.5		5.05		47.5		2750
20	9.75		7.525		68.75		1625
21	7.5		5.05		47.5		2750
22	5.25		2.575		26.25		3875
23	5.25		7.525		68.75		1625
24	7.5		5.05		90		2750
25	7.5		5.05		47.5		2750
26	7.5		5.05		47.5		2750
27	3		5.05		47.5		2750
28	12		5.05		47.5		2750
29	7.5		10		47.5		2750
30	7.5		5.05		47.5		2750
31	7.5		5.05		47.5		2750
32	7.5		0.1		47.5		2750
33	7.5		5.05		47.5		500
34	7.5		5.05		47.5		2750
35	7.5		5.05		5		2750
36	7.5		5.05		47.5		2750
37	7.5		5.05		47.5		2750
38	7.5		5.05		47.5		5000

added to 21 g titanium tetraethoxide and mixed vigorously for 15 min until titanium tetraethoxide completely penetrated into the resin structure. Then, 200 mL of 1 M ammonium hydroxide was added to the mixture and the

reflux operation was performed at 70 °C for 5 h. In the next step, the resin was washed with double distilled water until the solution pH approached 7. Finally, the prepared composite resin was dried overnight in a vacuum oven at 65 °C [25].

Batch experiments

The batch experiments were performed to determine the sorption behavior of Cr(VI) onto the Ti-XAD7 adsorbent. For this purpose, 100 mL Cr(VI) solutions at different concentrations from 500 to 5000 ppb were prepared in 250 mL beakers and 0.1–10 g adsorbent was added. pH was adjusted to the desired level by addition of 0.1 M NaOH and 0.1 M H_2SO_4. Then, the solution was mixed in a rotary shaker at 130 rpm and sampling was done at predetermined intervals (Table 1). in the next step, the solutions were passed through cellulose acetate filter with a diameter of 0.22 μm, and residual chromium was measured using the ICP-OES. The Cr(VI) adsorption capacity and removal efficiency were calculated according to the Eqs. [1 and 2]:

$$qe\ (mg/g) = \frac{(C_0 - C_e) \times V}{w} \quad (1)$$

$$\text{Removal efficiency}\% = \frac{(C_0 - C_e)}{C_0} \times 100 \quad (2)$$

Where q_e is the adsorption capacity of the absorbent (mg/g), w is the weight of adsorbent (g), V is the solution volume (mL), and C_e and C_0 are the final and initial concentration of Cr(VI) (mg/L).

Multivariate experimental design

RSM is an attractive technique for modeling and optimizing parameters affecting the adsorption process. In the present study, RSM based CCD was applied to investigate the effect of the optimization of vital factors, i.e. pH (X_1), adsorbent dose (X_2, g/L), contact time (X_3, min), and initial Cr concentration (X_4, mg/L), on adsorption [32]. A five-level-four-factor central composite design (CCD) with 38 runs of experiments was employed to study the effect of the factors on the response (Table 1). Also the number of total samples for comparison between efficiency of XAD7 and Ti-XAD7 for Cr(VI) adsorption were 76 samples (38 samples for each adsorbent). Eq. (3) illustrates the formula for converting original values of variables to their coded values:

$$Xi = \frac{X_i - X_0}{\Delta X_i} \quad (3)$$

Where X_i is the coded value of the independent variable, X_0 is the center point value of X_i, and ΔX is the step change value. After developed the experiments, empirical second-order polynomial model was applied to describe the effect of variables on the response (adsorption rate) [32]:

$$Y = \beta_0 \sum_{i=1}^{n} a_i x_i + \sum_{i=1}^{n} a_{ii} x_i^2 + \sum_{i=1}^{n-1} \sum_{j=2}^{n} a_{ij} x_i x_j + \varepsilon \quad (4)$$

Where Y is the predicted response, β_0 is the constant coefficient, X_i and X_j indicate the independent variables in the form of coded values, a_i, a_{ii} and a_{ij} are the regression coefficients, and ε is the random error. The R software (version 3.3.1) was used for CCD design and the related statistical analysis [33].

Adsorption isotherms

Nonlinear regression

Nonlinear regression can be a powerful alternative to linear regression because it offers the most flexible curve-fitting functionality. For nonlinear models, the sum of square must be minimized by an iterative method. The nonlinear regression line is the line that minimizes the sum of squared deviations of prediction (also called the sum of squares error). In nonlinear regression, goodness of fitness (GooF) is used after error analysis. The best set of parameters for each isotherm is selected using the sum of normalized error (SNE). In this research, four isotherms with two parameter (TWP), i.e. the Temkin, Langmuir, Dubinin-Radushkevich, and Freundlich, and four isotherms with three parameters (THP), i.e. Toth, Khan, Redlich-Peterson, and Sips, were fitted to explain adsorption processes at the equilibrium point (Table 2). Moreover, minimization of the eight different non-linear error functions (see Table 3) was done to determine isotherm parameters and examine different isotherm models. The solver add-in of Microsoft Excel® (version 2013) was employed to maximize the coefficient of determination to produce the best fitness to experimental data and minimize the error functions to estimate the coefficients of isotherm models. Goodness of fitness (GooF) was applied in order to recognize the optimum isotherm. Error functions values were taken into account to classify isotherm models from the best to the worst.

Sum of the normalized error (SNE)

A various set of parameters can be generated for each isotherm by various error functions [52]. In the current study, a normalization method was established to select the best set of parameters for each isotherm. In this regard, the selected parameters were obtained by calculating the sum of the normalized error (SNE) according to the following steps:

Table 2 Non-linear forms of adsorption isotherm and kinetic models

isotherm model	Equation	Parameters	Eqs	Reference
Langmuir	$q_e = \frac{Q_0 b C_e}{1+bC_e}$	$Q_0 = \frac{1}{\text{intercept}}$ $b = \frac{1}{\left(\frac{\text{slop}}{\text{intercept}}\right)}$	5	[2, 34]
Frundlich	$q_e = K_F C_e^{1/n}$	$n = \frac{1}{\text{slop}}$ $K_F = \exp(\text{intercept})$	6	[2, 35, 36]
Tempkin	$q_e = \frac{RT}{b_T} \ln A_T C_e$	$b_T = \frac{RT}{\text{slop}}$ $A_T = \exp\left(\frac{\text{intercept}}{\text{slop}}\right)$	7	[37]
Dubinin–Radushkevich	$q_e = (q_S)\exp(-k_{ad}\varepsilon^2)_e^{1/n}$	$q_s = \exp(\text{intercept})$ $K_{ad} = -\text{slop}$	8	[38, 39]
Sips	$q_e = \frac{q_s k_s c_e^{m_s}}{1+k_s c_e^{m_s}}$	–	9	[40]
Redlich-Peterson	$q_e = \frac{k_R c_e}{1+a_R c_e^{\beta}}$	–	10	[41]
Toth	$q_e = \frac{k_T c_e}{(a_T c_e)^{\frac{1}{t}}}$	–	11	[38]
Khan	$q_e = \frac{q_s b_k c_e}{(1+b_k c_e)^{a_k}}$	–	12	[42]
kinetic models	Equation	Parameters	Eqs	Reference
Pseudo-first-order	$q_t = q_e\,(1\text{-}e^{-k_1 t})$	$q_e = \exp(\text{intercept})$ $K_1 = -(\text{slop})$	13	[43]
Pseudo-second-order	$q_t = \frac{q_e^2 k_2 t}{1+q_e k_2 t}$	$q_e = \frac{1}{slop}$ $K_2 = \frac{slop^2}{intercept}$	14	[44]
Elovich	$q_t = \frac{\ln a_e\ b_e}{b_e} + \frac{1}{b_e} \ln t$	$ae = \exp\left(\frac{\text{intercept}}{\text{slop}} - \text{In}\, b_e\right)$ $b_e = \frac{1}{slop}$	15	[45]
Intraparticle diffusion	$q_t = k_i\, t^{\frac{1}{2}} + c$	$K_i = \text{slop}$ $C = \text{intercept}$	16	[46]

I) one isotherm and one error function were selected and the isotherm parameters were determined based on the trial and error method so that the obtained parameters minimized the selected error function.

II) the values of other error functions for obtained parameters of the selected isotherm were calculated.

III) the steps I and II were repeated for individual isotherms and other error functions.

IV) the ratio of associated error functions related to each parameter set to the largest associated error function were computed.

V) the obtained ratios for that parameter set were summed.

Table 3 Equations of error functions

Error function	Abbreviation	formula	Eq.	Ref.
Sum of the squares of the errors	ERRSQ/SSE	$\sum_{i=1}^{n}\left(q_{e,calc}-q_{e,exp}\right)_i^2$	17	[47]
Hybrid fractional error function	HYBRID	$\frac{100}{n-p}\sum_{i=1}^{n}\left[\frac{\left(q_{cal}-q_{exp}\right)^2}{q_{exp}}\right]$	18	[48]
Average relative error	ARE	$\frac{100}{n}\sum_{i=1}^{n}\left\lvert\frac{q_{e,exp}-q_{e,calc}}{q_{e,exp}}\right\rvert$	19	[34]
Sum of absolute error	EABS	$\sum_{i=1}^{n}\left\lvert q_{e,exp}-q_{e,calc}\right\rvert$	20	[49]
Marquardt's percent standard deviation	MPSD	$\sqrt[100]{\frac{1}{n-p}\sum_{i=1}^{n}\left(\frac{q_{e,exp}-q_{e,calc}}{q_{e,exp}}\right)_i^2}$	21	[34]
Nonlinear chi-square test	X^2	$\sum_{i=1}^{n}\frac{\left(q_{e,cal}-q_{e,exp}\right)^2}{q_{e,exp}}$	22	[50]
Residual Root Mean Square Error	RMSE	$\sqrt{\frac{1}{n-2}\sum_{i=1}^{n}\left(q_{e,exp}-q_{e,calc}\right)_i^2}$	23	[50]
Average Percentage Errors	APE	$\frac{\sum_{i=1}^{n}\left\lvert\frac{q_{e,exp}-q_{e,calc}}{q_{e,exp}}\right\rvert}{p}\times 100$	24	[51]

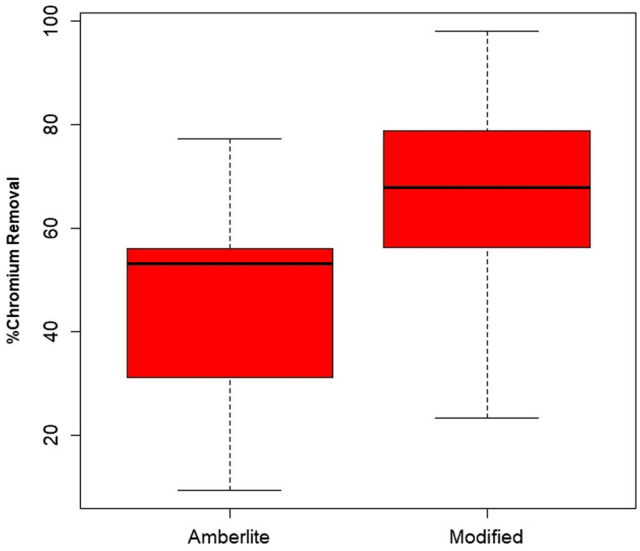

Fig. 1 Box plot of Cr (VI) removal efficiency by XAD7 and Ti-XAD7

VI) the parameter set with the minimum SNE was designated as the best set of parameters for that isotherm.

Adsorption kinetics

Nonlinear regression

Four kinetic models, including Elovich, Intraparticle diffusion, pseudo-first order, and pseudo-second order, were applied to fit the experimental data and obtain the best results. The nonlinear equations of kinetic models are presented in Table 2. The R-squared (R^2) was maximized to obtain the nonlinear kinetic models and select the best fitted model to the experimental data. The R^2 value was calculated as follows:

$$R2 = \frac{\sum_{i=1}^{n}\left(q_{e,calc}-\overline{q}_{e,exp}\right)_i^2}{\sum_{i=1}^{n}\left(q_{e,calc}-\overline{q}_{e,exp}\right)_i^2+\sum_{i=1}^{n}\left(q_{e,calc}-\overline{q}_{e,exp}\right)_i^2} \quad (25)$$

Where $q_{e,ccalc}$ is the calculated adsorption capacity, $\overline{q}_{e,exp}$ is the average of $q_{e,exp}$, and $q_{e,exp}$ is the experimental adsorption capacity.

Results and discussions

Comparison of adsorption efficiency

Figure 1 and Table 4 present the efficiency of XAD7 and Ti-XAD7 samples for chromium adsorption. The Ti-XAD7 was more efficient than Amberlite XAD7 in Cr(VI) removal. The

Table 4 Comparison of Cr (VI) removal efficiency for XAD7 and Ti-XAD7

Run	pH	Adsorbent dose	Contact time	Cr(VI) concentration	Removal efficiency of XAD7%	Removal efficiency of Ti-AD7%
1	7.5	5.05	47.5	2750	55.23	75.24
2	9.75	7.525	26.25	1625	49.31	71.44
3	9.75	7.525	26.25	3875	34.13	59.12
4	9.75	7.525	68.75	3875	42.47	63.22
5	5.25	2.575	26.25	1625	29.74	42.17
6	9.75	2.575	68.75	1625	45.56	72.2
7	5.25	7.525	26.25	3875	31.24	50.14
8	7.5	5.05	47.5	2750	55.17	76.28
9	9.75	2.575	26.25	3875	27.39	51.36
10	7.5	5.05	47.5	2750	54.93	77.62
11	5.25	7.525	26.25	1625	42.4	60.29
12	7.5	5.05	47.5	2750	54.3	78.84
13	5.25	2.575	68.75	1625	40.39	57.53
14	5.25	2.575	68.75	3875	31.17	47.39
15	9.75	2.575	68.75	3875	31.14	63.1
16	9.75	2.575	26.25	1625	39.65	64.21
17	5.25	7.525	68.75	3875	40.54	56.22
18	7.5	5.05	47.5	2750	56.05	75.49
19	7.5	5.05	47.5	2750	54.33	79.93
20	9.75	7.525	68.75	1625	53.7	62.38
21	7.5	5.05	47.5	2750	54.9	81.19
22	5.25	2.575	26.25	3875	23.52	33.44
23	5.25	7.525	68.75	1625	52.74	62.02
24	7.5	5.05	90	2750	69.19	91.14
25	7.5	5.05	47.5	2750	57.04	82.75
26	7.5	5.05	47.5	2750	56.18	74.57
27	3	5.05	47.5	2750	9.44	31.79
28	12	5.05	47.5	2750	55.7	61.7
29	7.5	10	47.5	2750	77.2	98.06
30	7.5	5.05	47.5	2750	56.19	72.42
31	7.5	5.05	47.5	2750	57.33	77.28
32	7.5	0.1	47.5	2750	12.5	23.2
33	7.5	5.05	47.5	500	67.36	90.2
34	7.5	5.05	47.5	2750	56.63	86.85
35	7.5	5.05	5	2750	14.2	25.4
36	7.5	5.05	47.5	2750	57.35	88.2
37	7.5	5.05	47.5	2750	56.44	84.19
38	7.5	5.05	47.5	5000	15.21	40.7

Wilcoxon test results (see Table 5) also confirmed that the Ti-XAD7 had a better performance (about 98%) compared to the XAD7 (nearly 80%) for Cr(VI) removal from aqueous solution. Therefore, due to the higher efficiency of Ti-XAD7, this adsorbent was used in the future section (Statistical analysis and model development) of this study.

Table 5 Comparison of Cr (VI) removal efficiency for XAD7 and Ti-XAD7

	adsorbant	
	XAD7	Ti-XAD7
Minimum	9.44	23.20
1st Qu.	31.96	56.55
Median	53.22	67.83
Mean	45.21	65.51
3rd Qu.	56.15	78.53
Maximum	77.20	98.06

Characterization of Ti-XAD7

The scanning electron microscope (SEM) images of the XAD7 Amberlite and Ti-XAD7 at 50.0 Kx magnification are shown in Fig 2 (a) and (b). The SEM images of XAD7 Amberlite resin indicated irregular morphological aggregation with large amounts of inter-particle voids, whereas Ti-XAD7 images showed that the degree of aggregation increased with loading TiO_2 on Amberlite [53]. It was observed that synthesized Ti-XAD7 had a porous and heterogeneous structure with a size range of 130-200 nm. The images indicated that the surface of the adsorbents was rough and had a decent porosity. This feature developed the contact between the Cr (VI) and Ti-XAD7 adsorbent, which resulted in the improvement of the adsorption performance.

Fourier-transform infrared spectroscopy (FTIR) of the original and TiO_2-loaded Amberlite XAD7 resin in the range of 4000–400 cm^{-1} is presented in Fig. 2.C. In both spectra, the hydroxyl group appeared at a broad band around 3420 cm^{-1}. The presence of strong bands at 1260 cm^{-1} and 1730 cm^{-1} in all samples was attributed to C–O stretching in ester and H-O-H bending in water molecules on the surface, respectively [54]. The peaks in the Ti-XAD7 spectrum at around 522

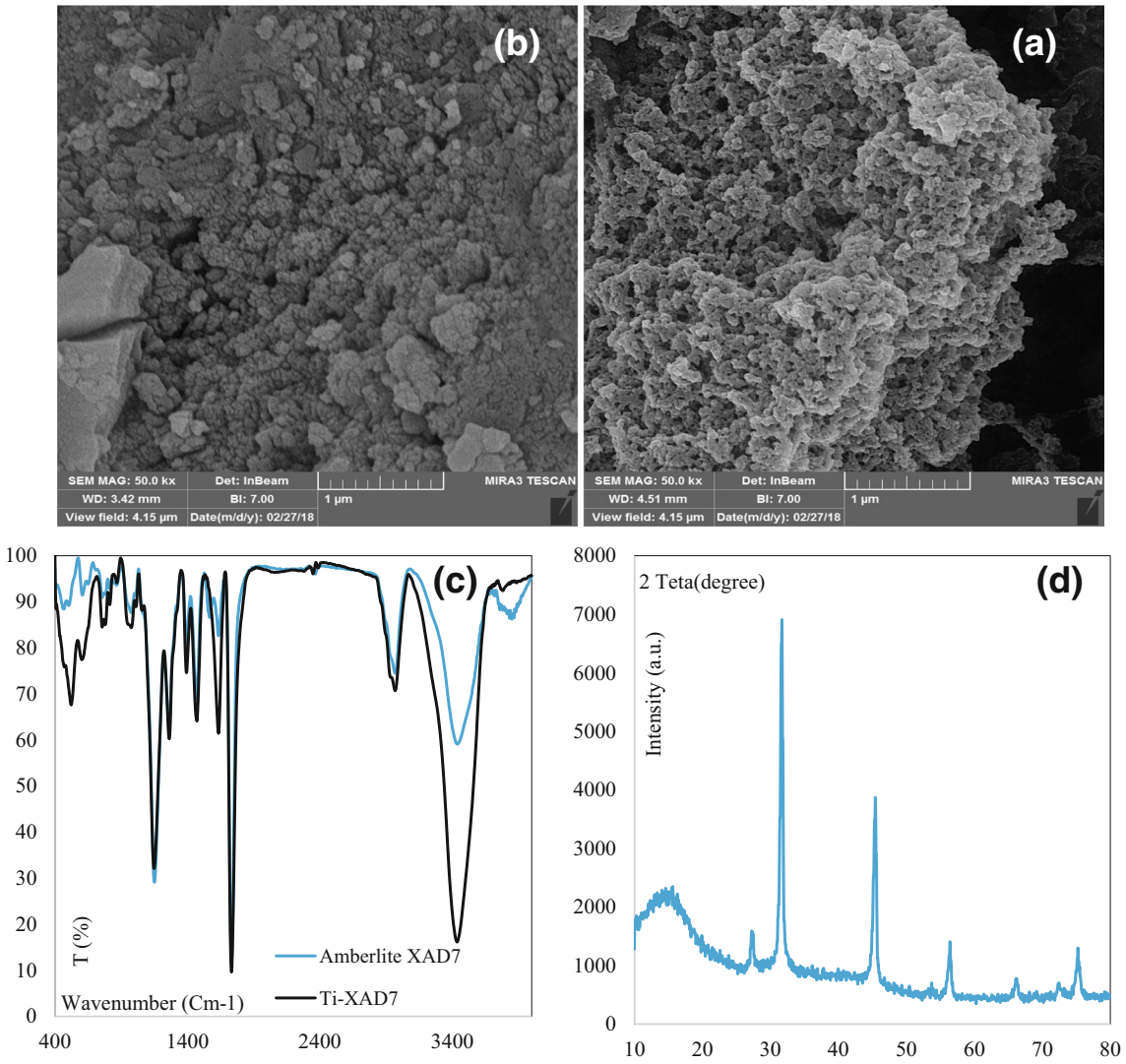

Fig. 2 SEM image of (a) Amberlite XAD7 and (b) Ti-XAD7, (c) FTIR images of Amberlite XAD7 and Ti-XAD7 and (d) XRD image Ti-XAD7

Table 6 Results of experimental design matrix for Cr(VI) adsorption by Ti-XAD7

Run	Actual level of factors (Coded variables)				Block	Y (%)
	X_1	X_2	X_3	X_4		
32	7.5(0)	0.1(−1)	47.5(0)	2750(0)	2	23.20
35	7.5(0)	5.05(0)	5(−1)	2750(0)	2	25.40
27	3.5(−1)	5.05(0)	47.5(0)	2750(0)	2	31.79
22	5.25(−0.5)	2.575(−0.5)	26.25(−0.5)	3875(0.5)	1	33.44
38	7.5(0)	5.05(0)	47.5(0)	5000(1)	2	40.70
5	5.25(−0.5)	2.575(−0.5)	26.25(−0.5)	1625(−0.5)	1	42.17
14	5.25(−0.5)	2.575(−0.5)	68.75(0.5)	3875(0.5)	1	47.39
7	5.25(−0.5)	7.525(0.5)	26.25(−0.5)	3875(0.5)	1	50.14
9	9.75(0.5)	2.575(−0.5)	26.25(−0.5)	3875(0.5)	1	51.36
17	5.25(−0.5)	7.525(0.5)	68.75(0.5)	3875(0.5)	1	56.22
13	5.25(−0.5)	2.575(−0.5)	68.75(0.5)	1625(−0.5)	1	57.53
3	9.75(0.5)	7.525(0.5)	26.25(−0.5)	3875(0.5)	1	59.12
11	5.25(−0.5)	7.525(0.5)	26.25(−0.5)	1625(−0.5)	1	60.29
28	12(1)	5.05(0)	47.5(0)	2750(0)	2	61.70
23	5.25(−0.5)	7.525(0.5)	68.75(0.5)	1625(−0.5)	1	62.02
20	9.75(0.5)	7.525(0.5)	68.75(0.5)	1625(−0.5)	1	62.38
15	9.75(0.5)	2.575(−0.5)	68.75(0.5)	3875(0.5)	1	63.10
4	9.75(0.5)	7.525(0.5)	68.75(0.5)	3875(0.5)	1	63.22
16	9.75(0.5)	2.575(−0.5)	26.25(−0.5)	1625(−0.5)	1	64.21
2	9.75(0.5)	7.525(0.5)	26.25(−0.5)	1625(−0.5)	1	71.44
6	9.75(0.5)	2.575(−0.5)	68.75(0.5)	1625(−0.5)	1	72.20
33	7.5(0)	5.05(0)	47.5(0)	500(−1)	2	90.20
29	7.5(0)	10(1)	47.5(0)	2750(0)	2	98.06
30	7.5(0)	5.05(0)	47.5(0)	2750(0)	2	72.42
26	7.5(0)	5.05(0)	47.5(0)	2750(0)	2	74.57
31	7.5(0)	5.05(0)	47.5(0)	2750(0)	2	77.28
25	7.5(0)	5.05(0)	47.5(0)	2750(0)	2	82.75
37	7.5(0)	5.05(0)	47.5(0)	2750(0)	2	84.19

X_1 = pH, X_2 = Adsorbent (g/L), X_3 = Time (min), X_4 = Cr(VI) concentration (ppb), Y = Removal efficiency of Ti-XAD7 (%).

cm^{-1} and 605 cm^{-1} were attributed to the Ti-O-Ti (Ti-O) and theoretical frequencies of Ti $(OC_2H_5)_4$ (600 to 623 cm^{-1}), respectively. The bands at 2971.62 cm^{-1} were related to the stretching and bending vibration of the C–H group in the resin structure. The bands at 1639.04 and 1384.68 cm^{-1} are usually attributed to the –OH bending vibrations of water molecules and/or the bond between oxygen in TiO_2 and hydrogen in the physical adsorbed water molecules. The above-mentioned

Table 7 Regression analysis for the reduced quadratic model of Cr(VI) removal by Ti-XAD7

Model term	Coefficient estimate	Std. error	t-value	p value
Intercept	72.0042	3.4589	20.8173	1.68×10^{-15}
X_1	13.1375	4.5657	2.8774	9.014×10^{-3}
X_2	16.9292	45,657	3.7079	1.303×10^{-3}
X_3	7.0697	5.3686	1.3169	0.202074
X_4	−13.9375	4.5657	−3.0526	6.047×10^{-3}
X_1^2	−24.0923	8.5682	−2.8118	1.0449×10^{-2}
X_3^2	−37.2007	11.3526	−3.2768	3.599×10^{-3}
$R^2 = 0.7251$, $R^2_{adj} = 0.6465$, p value: 5.221×10^{-05}				

X_1 = pH, X_2 = Adsorbent (g/L), X_3 = Time (min), X_4 = Cr(VI) concentration (ppb).

Table 8 Variance analysis (ANOVA) of the adsorption of Cr(VI) by Ti-XAD7

source	DF	Sum of squares	Mean of squares	F-value	Pr (>|t|)
FO(X_1,X_2,X_3,X_4)	4	4657.8	1164.44	9.3099	1.721×10^{-4}
PQ(X_1,X_3)	2	2269.3	1134.63	9.0716	1.4468×10^{-3}
Residuals	21	2626.6	125.07		
Lack of fit	17	2522.6	148.39	5.7069	5.19144×10^{-2}
Pure error	4	104	26		

X_1 = pH, X_2 = Adsorbent (g/L), X_3 = Time (min), X_4 = Cr(VI) concentration (ppb).

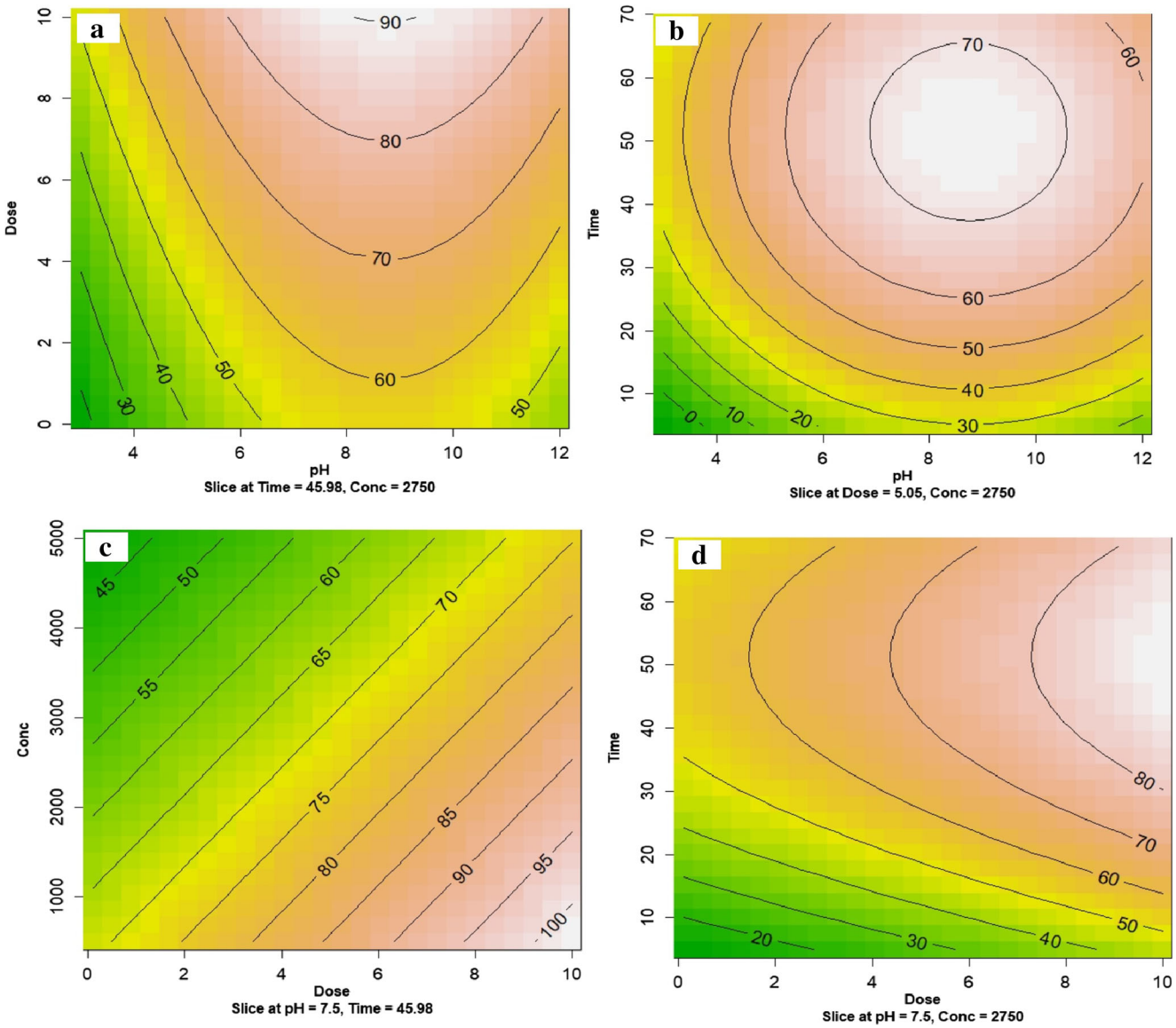

Fig. 3 Contour plots used to display the effects of, a: pH and adsorbent dose, b: time and pH, c: adsorbent dose and concentration, and d: time and adsorbent dose, for Ti-XAD7

Table 9 Optimization of factors based on the response surface modeling

	X_1	X_2	X_3	X_4
Ti-XAD7	8.7	5.05	51.53	2750

X_1 = pH, X_2 = Adsorbent (g/L), X_3 = Time (min), X_4 = Cr (VI) concentration (ppb).

results confirmed the proper loading of TiO_2 onto the Amberlite XAD-7 resin [22, 55].

X-ray diffraction (XRD) patterns of Ti-XAD7 in the range of 2θ=10–80° are shown in Fig. 2.d. The diffraction peaks at 27.46° for (1 0 1), 31.71° for (0 0 4), 45.45° for (2 0 0), 56.46° for (2 1 1), 66.31° for (116) and 75.26° for (220) based on JCPDS no. 21-1272 indicated the presence of TiO_2 with an anatase structure. The presence of other peaks, i.e. a broad peak at 15.11°, was attributed to XAD7 resin. Moreover, sharp peaks at 31.71° and 45.45° could be due to the overlapping of the iron in the resin structure and TiO_2 NPs [56].

Statistical analysis and model development of Cr(VI) adsorption on Ti-XAD7

It should be noted that 38 run were considered for the experiment. After performing the lab test for XAD7 it was shown that that quadratic model is the best choice. As there was not any indication for three or four ways interaction, the fractional CCD was considered for Ti-XAD7; to reduce the number of laboratory runs without any problem in the outcomes of modeling for two ways interactions. So, to investigate the effect of independent variables, including Cr(VI) concentration, contact time, pH, and adsorbent dosage, on adsorption of Cr(VI) by Ti-XAD7, 28 experiments were suggested using the CCD approach. According to Table 6, the highest and the lowest removal efficiency for Ti-XAD7 was around 98%, and 23%, respectively.

The results of RSM analysis, including standard error, t-value, and the significance of input variables for Cr(VI) removal by Ti-XAD7, are presented in Table 7. The impact of contact time on Cr(VI) removal by Ti-XAD7 was not statistically significant, while other factors (adsorbent dosage, pH, and Cr(VI) initial concentration) were effectively associated with Cr(VI) removal ($p < 0.05$). The p value, R^2, and adjusted R^2 (R^2_{adj}) were used to investigate the accuracy of the model. The model was found to be statistically significant (p value = 5.221×10^{-05}) and had a high R^2 value of 0.7251. Additionally, a small difference (0.0786) was found between the R^2 and R^2_{adj}, indicating a reasonable consistency of the quadratic model with the experimental data. As shown in Table 8, the model terms are divided into two categories: first order or linear terms (FO) and pure quadratic (PQ) terms. The results of ANOVA (Table 8) indicated that all first order parameters and pure quadratic terms included in the model were statistically significant. Model validation was also evaluated using the lack-of-fit parameter (LOF). The results showed a P value of 0.0519 for LOF, indicating a non-significant correlation (larger than 0.05) between the factors and the response.

Response surface and contour plots of parameters

The interaction between all investigated factors and Cr(VI) adsorption is shown in Fig. 3. An increase of the adsorbent dosage from 0.1 to 10 g/L increased the adsorption efficiency by increasing the pH from 3 to 12, as shown in Fig. 3a. When the adsorbent dosage and Cr(VI) initial concentration was fixed at 5.05 g/L and 2750 ppb respectively, the removal efficiency increased with an increase in pH to 9 for a determined contact time (for example 50 min) [Fig. 3b]. However, at a higher pH [9–12], an opposite effect was seen. At a contact time of 40 min, the removal efficiency was 70% and 60% at pH = 9 and 11, respectively. The results showed that the removal efficiency of Cr(VI) by Amberlite XAD7 resin loaded with titanium dioxide improved markedly when pH increased from 3 to 9. Figure 3c presents the interaction between the adsorbent dose and Cr(VI) initial concentrations. With a decrease in the Cr(VI) concentration from 5000 to 500 ppb, the adsorption efficiency improved by increasing the adsorbent dosage from 0.1 to 10 g/L. Figure 3d shows increased removal efficiency by increasing the contact time for a specified absorbent dosage (for example, 5 g/L) when pH and Cr(VI) initial concentration are fixed at their centerpoints.

Optimization of Cr(VI) adsorption process

The optimal parameters of the Cr(VI) adsorption by Ti-XAD7 were found based on mathematical equations. The Solver

Table 10 Ranking of two-parameter isotherm models for different error functions

RMSE	X^2	ERRSQ	HYBRID	MPSD	ARE	EABS	APE	Most visited
LA	DR	LA	DR	DR	LA	FR	LA	LA
FR	LA	FR	LA	LA	FR	TE	FR	FR
TE	FR	TE	FR	FR	TE	DR	TE	TE
DR	TE	DR	TE	TE	DR	LA	DR	DR

LA:Langmuir, FR:Frundlich, TE:Tempkin, DR:Dubinin-Radushkevich.

Table 11 Ranking of three-parameter isotherm models for different error functions

RMSE	X^2	ERRSQ	HYBRID	MPSD	ARE	EABS	APE	Most visited
SI	SI	SI	R-P	SI	SI	SI	SI	SI
R-P	R-P	R-P	TO	R-P	R-P	R-P	R-P	R-P
TO	TO	TO	KH	TO	KH	KH	KH	KH
KH	KH	KH	SI	KH	TO	TO	TO	TO

R-P: Redlich-Peterson, SI: Sips, KH: Khan, TO: Toth.

software was employed for maximization of the Cr(VI) adsorption to produce the optimum value for each factor. The optimum conditions of the four factors are shown in Table 9.

Adsorption isotherms

Selecting the best isotherm model

The results of the isotherm models ranking are shown in Tables 10, 11 and 12. The first rank belonged to the isotherm with the lowest error function. According to Table 10, according to the RMSE, ERRSQ, APE and ARE error functions, the best isotherm model was the Langmuir followed by Freundlich, Tempkin, and Dubinin-Radushkevich. According to χ^2, HYBRID and MPSD error functions, the best model was the Dubinin-Radushkevich followed by Langmuir, Freundlich and Tempkin. Based on the EABS error function, Freundlich was the best model followed by Tempkin, Dubinin-Radushkevich, and Langmuir. In the overall ranking (highlighted column), the Langmuir, Freundlich, Tempkin, and Dubinin-Radushkevich models ranked 1st to 4th based on the highest frequency of each isotherm in each row. Finally, the Langmuir isotherm model was selected as the best fitted nonlinear model for the data.

According to Table 11, based on the RMSE, χ^2, ERRSQ, and MPSD error functions, Sips was the best isotherm model followed by Redlich-Peterson, Toth, and Khan in order. According to ARE, EABS, and APE error functions, Sips was the best model followed by Redlich-Peterson, Khan, and Toth. Based on the HYBRID error function, Redlich-Peterson was the best model followed by Toth, Khan, and Sips. In overall ranking (highlighted column), the Sips, Redlich-Peterson, Khan, and Toth models ranked 1st to 4th based on the highest frequency of each isotherm in each row. Finally, the Sips isotherm model was selected as the best fitted nonlinear model for the data.

According to Table 12, as for overall ranking (highlighted column), Sips was the best isotherm model followed by Redlich-Peterson, Toth, Khan, Langmuir, Freundlich, Tempkin, and Dubinin-Radushkevich models based on the highest frequency of each isotherm in each row. Finally, the Sips isotherm model was selected as the best fitted nonlinear model for the data.

Determination of optimal parameter values by SNE method

Tables 13 and 14 show the coefficients of fitted TWP and THP isotherm models of the Cr(VI) adsorption on Ti-XAD7, which were obtained by minimizing various error functions. The optimal values of the parameters for each isotherm obtained from the standardized normal error method are shown in highlighted columns. According to Tables 13 and 14, as for Dubinin-Radushkevich ($K_{ad} = 1.8E\text{-}08$, $q_s = 1.39$) and Langmuir ($q_0 = 2.5$, $b = 1$) for TWP and Redlich-Peterson ($k_r = 2.85$, $a_r = 1.46$, $\beta = 0.79$) and Sips ($k_s = 1.86$, $q_s = 0.88$, $m_s = 0.59$) for THP adsorption isotherms, the optimal parameters were obtained by minimizing the MPSD error function. As for Tempkin ($b_T = 7519$, $a_T = 31.2$), adsorption by χ^2 error

Table 12 Ranking of TWP and THP isotherm models for different error functions

RMSE	X^2	ERRSQ	HYBRID	MPSD	ARE	EABS	APE	Most visited
SI	DR	SI	DR	DR	LA	SI	LA	SI
R-P	SI	R-P	R-P	SI	SI	R-P	SI	R-P
To	R-P	To	To	LA	R-P	Kh	R-P	To
Kh	To	Kh	Kh	R-P	Kh	To	Kh	Kh
LA	Kh	LA	LA	To	To	FR	FR	LA
FR	LA	FR	FR	Kh	FR	TE	To	FR
TE	FR	TE	SI	FR	TE	DR	TE	TE
DR	TE	DR	TE	TE	DR	LA	DR	DR

LA: Langmuir, FR: Frundlich, TE:Tempkin, DR: Dubinin-Radushkevich, SI: Sips, KH: Khan, TO: Toth, R-P: Redlich-Peterson.

Table 13 The constants of two-parameter isotherm obtained by different error function

Isotherm	Parameter	RMSE	X^2	ERRSQ	HYBRID	MPSD	ARE	EABS	APE
Langmuir	Q_0	2.73	2.63	2.73	2.63	2.50	2.49	2.49	2.49
	b	0.81	0.89	0.81	0.89	1.00	0.99	0.99	0.99
	R_L	0.076	0.070	0.076	0.070	0.063	0.063	0.063	0.063
Frundlich	K	1.06	0.98	1.06	0.98	0.96	1.03	0.98	1.03
	n	1.96	1.69	1.96	1.69	1.53	1.43	1.88	1.43
Tempkin	b_T	5724.1	7519.0	5724.2	7519.0	12,604.0	12,604.0	12,483.0	12,483.0
	A_T	21.1	31.2	21.1	31.2	45.4	50.1	49.9	49.9
Dubinin-Radushkevich	k_{ad}	4.1E-08	4.1E-08	4.1E-08	4.1E-08	1.8E-08	1.8E-08	4.1E-08	4.1E-08
	q_s	1.39	1.39	1.39	1.39	1.39	1.39	1.39	1.39

function yielded optimal parameters. Regarding Freundlich (k = 0.98, $n = 1.69$) for TWP and Toth ($k_T = 1.73$,$a_T = 0.6$, t = 1.28) and Khan ($b_k = 1.66$, $q_s = 1.55$, $a_k = 0.78$) for THP adsorption isotherms, optimal parameters were derived from the HYBRID error function. The Langmuir constant, b, which denotes adsorption energy, was 1 Lmg^{-1}. The high R^2 (near 1) obtained indicated a good agreement between the experimental values and isotherm parameters and also confirmed the monolayer adsorption of Cr(VI) onto the adsorbent surface. R_L, a dimensionless constant known as a quality determination factor of Langmuir isotherm, is presented in Eq. 26 [57].

$$RL = \frac{1}{1 + K_L C_0} \tag{26}$$

where K_L (b) and C_o are the Langmuir constant and the initial concentration of Cr(VI) ions in mg L^{-1}. The adsorption process was favorable within the range $0 < R_L < 1$, unfavorable when $R_L > 1$, became linear when $R_L = 1$, and was irreversible when $R_L = 0$. According to Table 12, the adsorption process was favorable for Ti-XAD7 because R_L ranged from 0 to 1. The strong interaction between the Cr(VI) molecules and the adsorbent can be explained by low relative factor of R_L [57].

In the Freundlich constant, $n > 1$ indicates favorable adsorption conditions [58]. On the other hand, the coefficient of determination obtained from the Freundlich isotherm model was 0.981, which was lower than the coefficient obtained from the Langmuir isotherm model (R^2 = 0.998), indicating that the equilibrium data were not fitted well with the Freundlich isotherm model.

The Langmuir isotherm model has been also used to present the best fit for the sorption of heavy metals, i.e. chromium ions onto/by a magnetic ion exchange resin [59], Lewatit FO36 nano ion exchange resin [60], Ulmus leaves and their ash [61], titan yellow-impregnated XAD-7 resin beads [22], and Amberlite IRA 410 [42].

Figures 4 and 5 present the plots of different nonlinear isotherm models with optimized values of the constants for defining the parameters of the isotherm models. According to these curves, the Langmuir model had the best fit on the experimental data among the four TWP isotherms. The lowest consistency was related to the Dubinin-Radushkevich isotherm. Regarding the three-

Table 14 The constants of three-parameter isotherm obtained by different error function

Isotherm	Parameter	RMSE	X2	ERRSQ	HYBRID	MPSD	ARE	EABS	APE
Sips	k_s	1.97	1.99	1.97	1.99	1.86	1.88	1.88	1.88
	q_s	0.89	0.90	0.89	0.90	0.88	0.86	0.86	0.86
	m_s	0.65	0.66	0.65	0.66	0.59	0.60	0.60	0.60
Redlich-Peterson	K_R	2.61	2.68	2.61	2.68	2.85	3.31	3.31	3.31
	a_R	1.18	1.25	1.18	1.25	1.46	1.88	1.88	1.88
	β	0.88	0.86	0.88	0.86	0.79	0.76	0.76	0.76
Toth	K_T	1.87	1.73	1.87	1.73	1.52	1.51	1.51	1.51
	a_T	0.71	0.60	0.71	0.60	0.45	0.44	0.44	0.44
	t	1.22	1.28	1.22	1.28	1.41	1.40	1.40	1.40
Khan	q_s	1.76	1.55	1.76	1.55	1.20	1.26	1.26	1.26
	b_K	1.41	1.66	1.41	1.66	2.23	2.34	2.34	2.34
	a_K	0.82	0.78	0.82	0.78	0.71	0.74	0.74	0.74

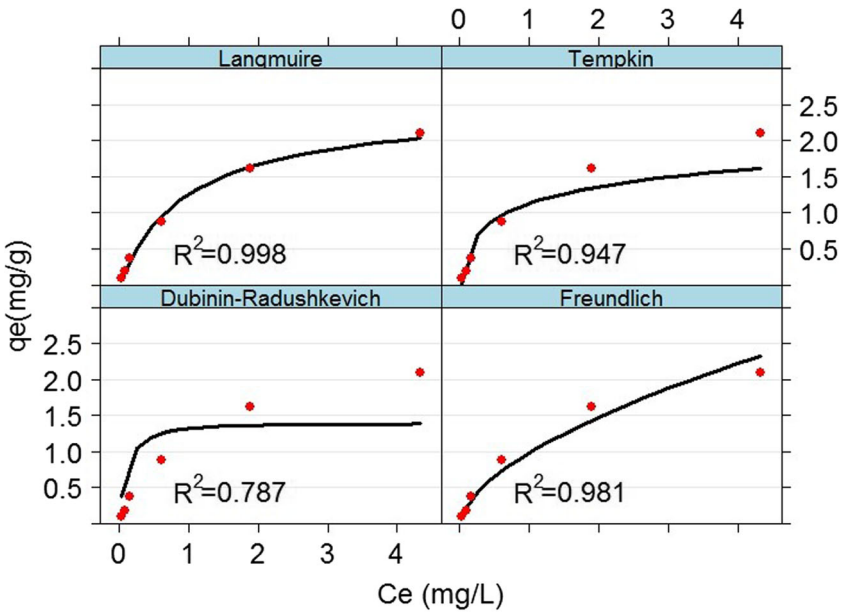

Fig. 4 Non-linear plot of two-parameter isotherm models fitted to the experimental data (T = 293 K, pH = 8.7, Ti-XAD7 dosage = 5.05 g/L, time = 120 min)

parameter models in Fig. 5, the non-linear regression curves and laboratory data were very compatible. Typically, if the number of model parameters is increased, the error of the fitting is decreased because the model fits better. Therefore, in the three-parameter models it is expected that the predicted values be more close to the experimental values. This causes these models to have a high coefficient of determination (R^2).

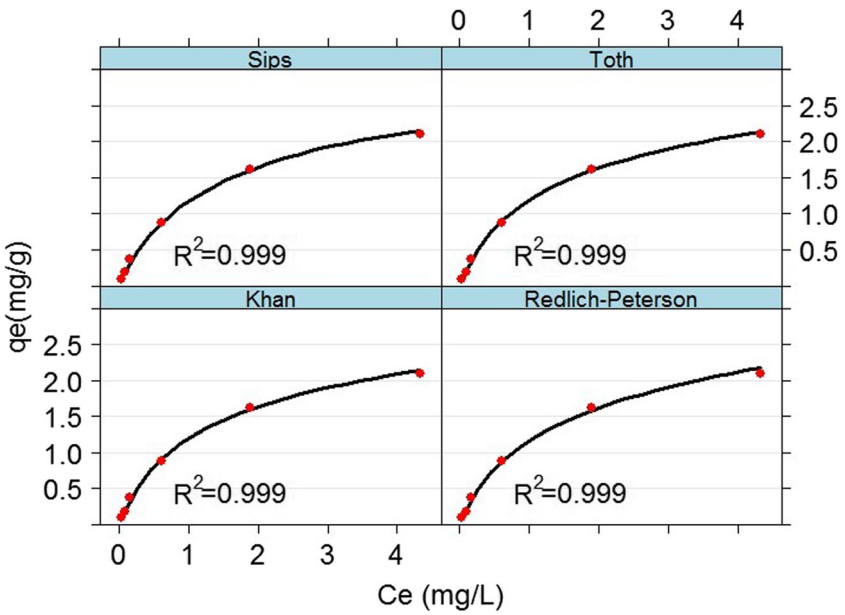

Fig. 5 Non-linear plot of three-parameter isotherm models fitted to the experimental data (T = 293 K, pH = 8.7, Ti-XAD7 dosage = 5.05 g/L, time = 120 min)

Table 15 Kinetic parameters for the Cr(VI) removal via Ti-XAD7 (T = 293 K, pH = 8.7, Ti-XAD7 dosage = 5.05 g/L)

Kinetic model	Parameter	Initial Concentration (mg/L) 2.75
Pseudo-first-order	q_e (mg/g)	0.245
	K_1 (1/min)	0.039
	R^2	0.931
Pseudo-second-order	q_e (mg/g)	0.285
	K_2 (g/mg min)	0.173
	R^2	0.960
Elovich	a_e (mMol/g min)	0.714
	b_e (g/m Mol)	0.552
	R^2	0.978
Intraparticle diffusion	k_i (mg/g $min^{1/2}$)	0.025
	C_i (mg/g)	1
	R^2	0.935

Adsorption kinetics

In this study, four different kinetic models (Elovich, Intraparticle diffusion, pseudo-first-order, and pseudo-second-order) were applied to test the kinetic data. The best fitted equation was identified by applying the R-squared (R^2). The model with the highest R^2 value was selected as the best model. Table 15 shows the kinetic constants and R^2 values obtained by the nonlinear method.

As a result, when the initial concentration of Cr(VI) was 2.75 mg/L, the Elovich model was the best model. On the other hand, the pseudo-first-order model with the lowest R^2 value was selected as the worst model (see Fig. 6). The significant difference between the q_0 value obtained from the Langmuir model (2.7 mg/g) and q_e value obtained from the pseudo-second order and pseudo-first order (0.285 and 0.245 mg/g, respectively) can indicate that chromium adsorption onto Ti-XAD7 is not controlled by the perfect pseudo-second or pseudo-first order reaction [62]. The assumption of the Elovich model is based on the presence of the heterogeneous active sites on the adsorbent that are related to the activation energy for chemisorption [62]. The adsorption kinetics at this initial concentration of Cr(VI) followed the Elovich model with a high correlation coefficient (0.978). The kinetic results of this study were consistent with adsorption of Cr ions onto various adsorbents such as the powder of potato peelings as a low cost sorbent [63], and aluminosilicate minerals in their Pb-exchanged forms [64].

Conclusions

According to the results, Cr(VI) was successfully removed from aqueous solution by Ti-XAD7. CCD and RSM were used for process modeling and optimization. The optimum conditions of initial Cr(VI) concentration, contact time, pH, and Ti-XAD7 dosage for the adsorption process were 2750 ppb, 51.53 min, 8.7, and 5.05 g/L, respectively. According to the results, chromium can be removed by this

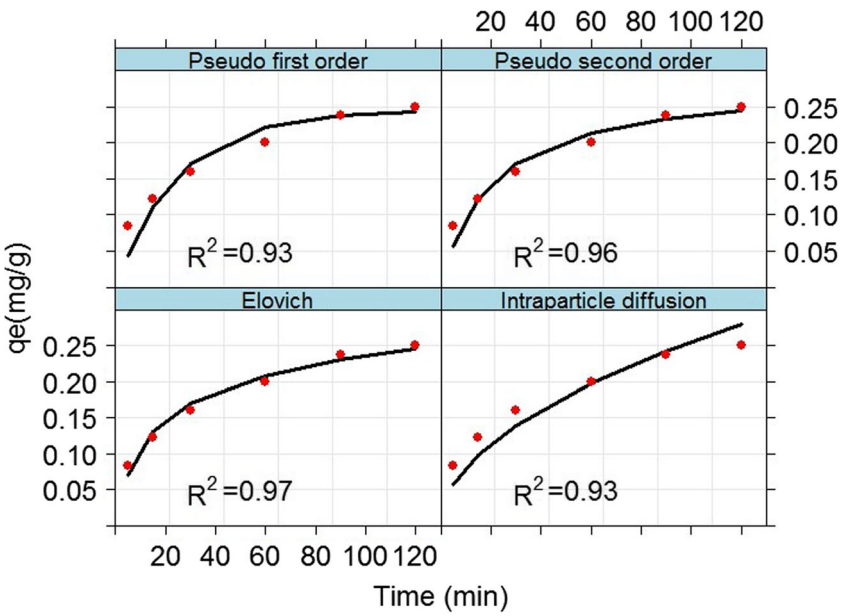

Fig. 6 Plot of adsorption kinetic equations for sorption of Cr(VI) onto Ti-XAD7 (T = 293 k, pH = 8.7, dosage = 5.05 g/L)

adsorbent at pH >7. Thus, the adsorbent can remove Cr(VI) without pH change. In summary, Ti-XAD7 is efficient compared with XAD7 for Cr(VI) removal from aqueous solutions.

Acknowledgements This work was a part of a research project financially supported by National Institute for Medical Research Development (NIMAD). The authors would like to thank NIMAD (Grant No 958367) and all the staff in the Chemistry Laboratory of the Department of Environmental Health Engineering for their assistance.

Compliance with ethical standards

Conflict of interest The authors of this article declare that they have no conflict of interests.

References

1. Kan C-C, Ibe AH, Rivera KKP, Arazo RO, de Luna MDG. Hexavalent chromium removal from aqueous solution by adsorbents synthesized from groundwater treatment residuals. Sustain Environ Res. 2017;27(4):163–71.
2. Albadarin AB, Mangwandi C, Ala'a H, Walker GM, Allen SJ, Ahmad MNM. Kinetic and thermodynamics of chromium ions adsorption onto low-cost dolomite adsorbent. Chem Eng J. 2012;179:193–202.
3. Pandikumar A, Ramaraj R. Photocatalytic reduction of hexavalent chromium at gold nanoparticles modified titania nanotubes. Mater Chem Phys. 2013;141(2–3):629–35.
4. Dwivedi AD, Permana R, Singh JP, Yoon H, Chae KH, Chang Y-S, et al. Tunichrome mimetic matrix, its perspective in abatement for carcinogenic hexavalent chromium and specific coordination behavior. Chem Eng J. 2017;328:629–38.
5. Wu Y, Song S, Garbers-Craig AM, Xue Z. Formation and leachability of hexavalent chromium in the Al2O3-CaO-MgO-Cr2O3 system. J Eur Ceram Soc. 2018;38(6):2649–61.
6. Kim C, Lee CR, Song YE, Heo J, Choi SM, Lim D-H, et al. Hexavalent chromium as a cathodic electron acceptor in a bipolar membrane microbial fuel cell with the simultaneous treatment of electroplating wastewater. Chem Eng J. 2017;328:703–7.
7. Stylianou S, Simeonidis K, Mitrakas M, Zouboulis A, Ernst M, Katsoyiannis IA. Reductive precipitation and removal of Cr (VI) from groundwaters by pipe flocculation-microfiltration. Environ Sci Pollut Res Int 2017:1–7.
8. Mortazavian S, An H, Chun D, Moon J. Activated carbon impregnated by zero-valent iron nanoparticles (AC/nZVI) optimized for simultaneous adsorption and reduction of aqueous hexavalent chromium: material characterizations and kinetic studies. Chem Eng J. 2018;353:781–95.
9. Yang Y, Chen N, Feng C, Li M, Gao Y. Chromium removal using a magnetic corncob biochar/polypyrrole composite by adsorption combined with reduction: reaction pathway and contribution degree. Colloids Surf A Physicochem Eng Asp. 2018;556:201–9.
10. Jahangiri K, Yousefi N, Ghadiri SK, Fekri R, Bagheri A, Talebi SS. Enhancement adsorption of hexavalent chromium onto modified fly ash from aqueous solution; optimization; isotherm, kinetic and thermodynamic study. J Dispers Sci Technol. 2019;40(8):1147–58.
11. Kakavandi B, Kalantary RR, Farzadkia M, Mahvi AH, Esrafili A, Azari A, et al. Enhanced chromium (VI) removal using activated carbon modified by zero valent iron and silver bimetallic nanoparticles. J Environ Health Sci Eng. 2014;12(1):115.
12. Asgari A, Vaezi F, Nasseri S, Dördelmann O, Mahvi A, Fard ED. Removal of hexavalent chromium from drinking water by granular ferric hydroxide. J Environ Health Sci Eng. 2008;5(4):277–82.
13. Mahvi AH, Nabizadeh R, Gholami F, Khairi A. Adsorption of chromium from wastewater by Platanus orientalis leaves. J Environ Health Sci Eng. 2007;4(3):191–6.
14. Golbaz S, Jafari AJ, Rafiee M, Kalantary RR. Separate and simultaneous removal of phenol, chromium, and cyanide from aqueous solution by coagulation/precipitation: mechanisms and theory. Chem Eng J. 2014;253:251–7.
15. Heidmann I, Calmano W. Removal of Cr (VI) from model wastewaters by electrocoagulation with Fe electrodes. Sep Purif Technol. 2008;61(1):15–21.
16. Assadi A, Dehghani MH, Rastkari N, Nasseri S, Mahvi AH. Photocatalytic reduction of hexavalent chromium in aqueous solutions with zinc oxide nanoparticles and hydrogen peroxide. Environ Prot Eng. 2012;38(4):5–16.
17. Kusku O, Rivas BL, Urbano BF, Arda M, Kabay N, Bryjak M. A comparative study of removal of Cr (VI) by ion exchange resins bearing quaternary ammonium groups. J Chem Technol Biotechnol. 2014;89(6):851–7.
18. Mihçiokur H, Peker İ. Batch study and kinetics of hexavalent chromium removal from aqueous solutions by anion exchange resin (Dowex 21 KCl). Desalination Water Treat. 2013;51(10–12):2116–20.
19. Hosseini-Bandegharaei A, Karimzadeh M, Sarwghadi M, Heydarbeigi A, Hosseini SH, Nedaie M, et al. Use of a selective extractant-impregnated resin for removal of Pb (II) ion from waters and wastewaters: kinetics, equilibrium and thermodynamic study. Chem Eng Res Des. 2014;92(3):581–91.
20. Hosseini-Bandegharaei A, Hosseini MS, Sarw-Ghadi M, Zowghi S, Hosseini E, Hosseini-Bandegharaei H. Kinetics, equilibrium and thermodynamic study of Cr (VI) sorption into toluidine blue o-impregnated XAD-7 resin beads and its application for the treatment of wastewaters containing Cr (VI). Chem Eng J. 2010;160(1):190–8.
21. Saha B, Gill RJ, Bailey DG, Kabay N, Arda M. Sorption of Cr (VI) from aqueous solution by Amberlite XAD-7 resin impregnated with Aliquat 336. React Funct Polym. 2004;60:223–44.
22. Hosseini-Bandegharaei A, Allahabadi A, Rahmani-Sani A, Rastegar A, Khamirchi R, Mehrpouyan M, et al. Thorium removal from weakly acidic solutions using titan yellow-impregnated XAD-7 resin beads: kinetics, equilibrium and thermodynamic studies. J Radioanal Nucl Chem. 2016;309(2):761–76.
23. Van Nguyen N. Lee J-c, Huynh HT, Jeong J. extraction and separation of cadmium from the chloride solution of E-waste using Cyanex 923 impregnated Amberlite XAD-7HP resin. Mater Trans. 2015;56(8):1294–301.
24. Haron MJ, Shiah LL, Wmz WY. Sorption of arsenic (V) by titanium oxide loaded poly (Hydroxamic acid) resin. Malaysian J Anal Sci. 2006;10(2):261–8.
25. Balaji T, Matsunaga H. Adsorption characteristics of as (III) and as (V) with titanium dioxide loaded Amberlite XAD-7 resin. Anal Sci. 2002;18(12):1345–9.
26. Parida K, Mishra KG, Dash SK. Adsorption of toxic metal ion Cr (VI) from aqueous state by TiO2-MCM-41: equilibrium and kinetic studies. J Hazard Mater. 2012;241:395–403.
27. Singh NB, Nagpal G, Agrawal S. Water purification by using adsorbents: a review. Environ Technol Inno. 2018.
28. Guan B, Lu W, Fang J, Cole RB. Characterization of synthesized titanium oxide nanoclusters by MALDI-TOF mass spectrometry. J Am Soc Mass Spectrom. 2007;18(3):517–24.
29. Bellifa A, Pirault-Roy L, Kappenstein C, Choukchou-Braham A. Study of effect of chromium on titanium dioxide phase transformation. B Mater Sci. 2014;37(3):669–77.

30. Zhang L, Zhang Y. Adsorption characteristics of hexavalent chromium on HCB/TiO2. Appl Surf Sci. 2014;316:649–56.
31. Krasucka P, Zaleski R, Skrzypiec K, Goworek J. Amberlite XAD copolymers as an environment for silica deposition. Micropor Mesopor Mat. 2017;237:210–21.
32. Cao J, Wu Y, Jin Y, Yilihan P, Huang W. Response surface methodology approach for optimization of the removal of chromium (VI) by NH2-MCM-41. J Taiwan Inst Chem Eng. 2014;45(3): 860–8.
33. Aslani H, Nabizadeh R, Nasseri S, Mesdaghinia A, Alimohammadi M, Mahvi AH, et al. Application of response surface methodology for modeling and optimization of trichloroacetic acid and turbidity removal using potassium ferrate (VI). Desalination Water Treat. 2016;57(52):25317–28.
34. Foo KY, Hameed BH. Insights into the modeling of adsorption isotherm systems. Chem Eng J. 2010;156(1):2–10.
35. Krishni RR, Foo KY, Hameed BH. Adsorption of methylene blue onto papaya leaves: comparison of linear and nonlinear isotherm analysis. Desalination Water Treat. 2014;52(34–36):6712–9.
36. Shokoohi R, Saghi MH, Ghafari HR, Hadi M. Biosorption of iron from aqueous solution by dried biomass of activated sludge. Iranian J Environ Health Sci Eng. 2009;6(2):107–14.
37. Gupta S, Babu BV. Removal of toxic metal Cr (VI) from aqueous solutions using sawdust as adsorbent: equilibrium, kinetics and regeneration studies. Chem Eng J. 2009;150(2–3):352–65.
38. Brdar M, Šćiban M, Takači A, Došenović T. Comparison of two and three parameters adsorption isotherm for Cr (VI) onto Kraft lignin. Chem Eng J. 2012;183:108–11.
39. Sepehr MN, Amrane A, Karimaian KA, Zarrabi M, Ghaffari HR. Potential of waste pumice and surface modified pumice for hexavalent chromium removal: characterization, equilibrium, thermodynamic and kinetic study. J Taiwan Inst Chem Eng. 2014;45(2):635–47.
40. L-g Y, L-l Q, Yu H-q, Li S, Shan R-R, Du B. Adsorption of acid dyes from aqueous solution by CTMAB modified bentonite: kinetic and isotherm modeling. J Mol Liq. 2015;211:1074–81.
41. Chan LS, Cheung WH, Allen SJ, McKay G. Error analysis of adsorption isotherm models for acid dyes onto bamboo derived activated carbon. Chin J Chem Eng. 2012;20(3):535–42.
42. Yasmine AO, Malika C, Abdeltif A, Aicha B. Sorption of hexavalent chromium metal onto Amberlite IRA 410–equilibrium isotherms and kinetic studies. Desalination Water Treat. 2012;38(1–3):409–15.
43. Elmorsi TM, Elsayed MH, Bakr MF. Enhancing the removal of methylene blue by modified ZnO nanoparticles: kinetics and equilibrium studies. Can J Chem. 2017;95(5):590–600.
44. Gusain D, Srivastava V, Sillanpää M, Sharma YC. Kinetics and isotherm study on adsorption of chromium on nano crystalline iron oxide/hydroxide: linear and nonlinear analysis of isotherm and kinetic parameters. Res Chem Intermediat. 2016;42(9):7133–51.
45. Babaei AA, Baboli Z, Jaafarzadeh N, Goudarzi G, Bahrami M, Ahmadi M. Synthesis, performance, and nonlinear modeling of modified nano-sized magnetite for removal of Cr (VI) from aqueous solutions. Desalination Water Treat. 2015;53(3):768–77.
46. Mohamed A, Nasser WS, Osman TA, Toprak MS, Muhammed M, Uheida A. Removal of chromium (VI) from aqueous solutions using surface modified composite nanofibers. J Colloid Interface Sci. 2017;505:682–91.
47. Fil BA, Korkmaz M, Özmetin C. Application of nonlinear regression analysis for methyl violet (MV) dye adsorption from solutions onto illite clay. J Dispers Sci Technol. 2016;37(7):991–1001.
48. Sreńscek-Nazzal J, Narkiewicz U, Morawski AW, Wróbel RJ, Michalkiewicz B. Comparison of optimized isotherm models and error functions for carbon dioxide adsorption on activated carbon. J Chem Eng Data. 2015;60(11):3148–58.
49. Shahmohammadi-Kalalagh S, Babazadeh H. Isotherms for the sorption of zinc and copper onto kaolinite: comparison of various error functions. Int J Environ Sci Technol. 2014;11(1):111–8.
50. Sivarajasekar N, Baskar R. Adsorption of basic red 9 onto activated carbon derived from immature cotton seeds: isotherm studies and error analysis. Desalination Water Treat. 2014;52(40–42):7743–65.
51. Hadi M, Samarghandi MR, McKay G. Equilibrium two-parameter isotherms of acid dyes sorption by activated carbons: study of residual errors. Chem Eng J. 2010;160(2):408–16.
52. Ofomaja AE, Ho Y-S. Effect of temperatures and pH on methyl violet biosorption by Mansonia wood sawdust. Bioresour Technol. 2008;99(13):5411–7.
53. Ullah I, Haider A, Khalid N, Ali S, Ahmed S, Khan Y, et al. Tuning the band gap of TiO 2 by tungsten doping for efficient UV and visible photodegradation of Congo red dye. Spectrochim Acta A 2018.
54. Draa MT, Belaid T, Benamor M. Extraction of Pb (II) by XAD7 impregnated resins with organophosphorus extractants (DEHPA, IONQUEST 801, CYANEX 272). Sep Purif Technol. 2004;40(1): 77–86.
55. Ignatyev IS, Montejo M, González JJL. DFT predictions of vibrational spectra of titanium tetramethoxide oligomers and the structure of titanium tetraalkoxides in liquid and solid phases. Vib Spectrosc. 2009;51(2):218–25.
56. Qian L, Ming M, Yuqing ZHA. Preparation and characterization of nanostructured au/TiO2 catalyst with high thermal stability. Chinese J Catal. 2006;27(12):1111–6.
57. Owalude SO, Tella AC. Removal of hexavalent chromium from aqueous solutions by adsorption on modified groundnut hull. Beni-suef Univer J Basic Appl Sci. 2016;5(4):377–88.
58. Srivastava V, Shekhar M, Gusain D, Gode F, Sharma YC. Application of a heterogeneous adsorbent (HA) for the removal of hexavalent chromium from aqueous solutions: kinetic and equilibrium modeling. Arab J Chem. 2017;10:S3073–S83.
59. Hans R, Senanayake G, Dharmasiri LCS, Mathes JAP, Kim DJ. A preliminary batch study of sorption kinetics of Cr (VI) ions from aqueous solutions by a magnetic ion exchange (MIEX®) resin and determination of film/pore diffusivity. Hydrometallurgy. 2016;164: 208–18.
60. Rafati L, Mahvi AH, Asgari AR, Hosseini SS. Removal of chromium (VI) from aqueous solutions using Lewatit FO36 nano ion exchange resin. Int J Environ Sci Technol. 2010;7(1):147–56.
61. Mahvi AH, Gholami F, Nazmara S. Cadmium biosorption from wastewater by Ulmus leaves and their ash. Eur J SciRes. 2008;23(2):197–203.
62. Mirzaei N, Ghaffari HR, Sharafi K, Velayati A, Hoseindoost G, Rezaei S, et al. Modified natural zeolite using ammonium quaternary based material for acid red 18 removal from aqueous solution. J Environ Chem Eng. 2017;5(4):3151–60.
63. Mutongo F, Kuipa O, Kuipa PK. Removal of Cr (VI) from aqueous solutions using powder of potato peelings as a low cost sorbent. Bioinorg Chem Appl 2014;2014.
64. Thanos AG, Katsou E, Malamis S, Drakopoulos V, Paschalakis P, Pavlatou EA, et al. Cr (VI) removal from aqueous solutions using aluminosilicate minerals in their Pb-exchanged forms. Appl Clay Sci. 2017;147:54–62.